Facile Preparation of Cationic Gold Nanoparticle-Bioconjugates for Cell Penetration and Nuclear Targeting

Isaac Ojea-Jiménez,[†,⊥,*] Lorena García-Fernández,[†,∥,⊥] Julia Lorenzo,[‡] and Victor F. Puntes[†,∥,§,*]

[†]Institut Català de Nanotecnologia (ICN), Campus UAB, 08193, Cerdanyola del Vallés, Spain, [∥]Universitat Autònoma de Barcelona (UAB), Campus UAB, 08193 Cerdanyola del Vallés, Spain, [‡]Institut de Biotecnologia i Biomedicina and Departament de Bioquímica i de Biologia Molecular, Universitat Autònoma de Barcelona, 08193 Cerdanyola del Vallés, Spain, and [§]Institució Catalana de Recerca i Estudis Avançats (ICREA), 08093, Barcelona, Spain. [⊥]Both authors have equally contributed to this work.

ABSTRACT The present work faces the rising demand of cationic particles of different sizes for biological applications, especially in gene therapies and nanotoxicology studies. A simple phase-transfer methodology has been developed for the functionalization of gold nanoparticles (Au NPs) with a variety of ligands, both cationic and anionic in aqueous solution, employing different nanocrystal sizes with narrow size distributions. Successful functionalization has been demonstrated by UV–vis spectroscopy, DLS, ζ-potential, and FTIR spectroscopy characterization of the particles before and after the phase transfer. The intracellular uptake of the differently charged Au NPs functionalized with peptidic biomolecules was investigated with human fibroblasts (1BR3G) by ICP-MS analysis of the digested cells and confocal fluorescence microscopy, which showed increased internalization of the cationic bioconjugates. Nuclear targeting could be observed by TEM, suggesting that the cationic peptidic biomolecule is acting as a nuclear localization signal.

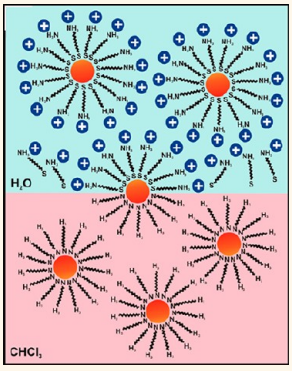

KEYWORDS: gold nanoparticles · surface chemistry · cationic particles · phase transfer · peptide · cell internalization

In the field of bionanotechnology for biomedical applications (*e.g.*, diagnosis and therapy),[1,2] the type of biological structures that can be targeted by NPs,[3] *i.e.*, in reaching the cytoplasm, crossing the nuclear membrane, or addressing particular cellular receptors, are primarily determined by their size,[4] shape, and surface functionalization.[5,6] In particular, the surface charge of NP-conjugates plays a critical role in determining the molecular interactions of NPs with their target cells. These interactions could, in turn, determine intracellular uptake and localization of the NPs, as well as their biological functions.[7] Although in principle the negative membrane potential of cells likely interacts more efficiently with cationic particles due to electrostatic interactions,[8,9] the formation of a protein corona and the evolution of the NP–protein complex must also be taken into account.[10] Cationic Au NPs have therefore attracted great interest in recent years for transfecting molecules into cells[11–15] and for drug delivery applications.[16,17] Unfortunately, there are few studies that conjugated positively charged ligand molecules as effectively as their anionic counterparts do to Au NPs.[18] Among the cationic ligands, a few reports can be found of lipids,[12,19] synthetic polymers such as poly(ethyleneimine)[20] or poly(allylamine),[7] aminoalkanethiols,[13,21–23] and quaternary ammonium salts[24,25] decorating the surface of Au NPs.

The most direct approach for the synthesis and cationic functionalization of Au NPs is the one performed in aqueous solution upon $NaBH_4$ reduction in the presence of cationic ligands.[12,13,19,21] This method is limited to a certain number of ligands, since others undergo reduction or decomposition by the strong reductive environment. Alternatively, the Brust–Schiffrin two-phase methodology makes use of a phase-transfer process to prepare small Au NPs coated with alkanethiolate monolayers by simply varying the thiol–gold stoichiometry.[26] The particles can be repeatedly isolated from and redissolved in common organic solvents without irreversible agglomeration or decomposition. Subsequent studies have shown that a wide range of alkanethiolate ligands can be employed in this same protocol[27,28] and also that the initial monolayer-protected clusters can be readily modified through ligand place-exchange reactions.[29,30] However, this method is restricted to very small particle sizes (from 1.5 to 6 nm). This strategy has largely been used by Rotello and co-workers in order to conjugate cationic aminoalkanethiols,[17,22]

* Address correspondence to isaac.ojea@icn.cat, victor.puntes@icn.cat.

Received for review March 19, 2012 and accepted August 7, 2012.

Published online August 07, 2012
10.1021/nn3012042

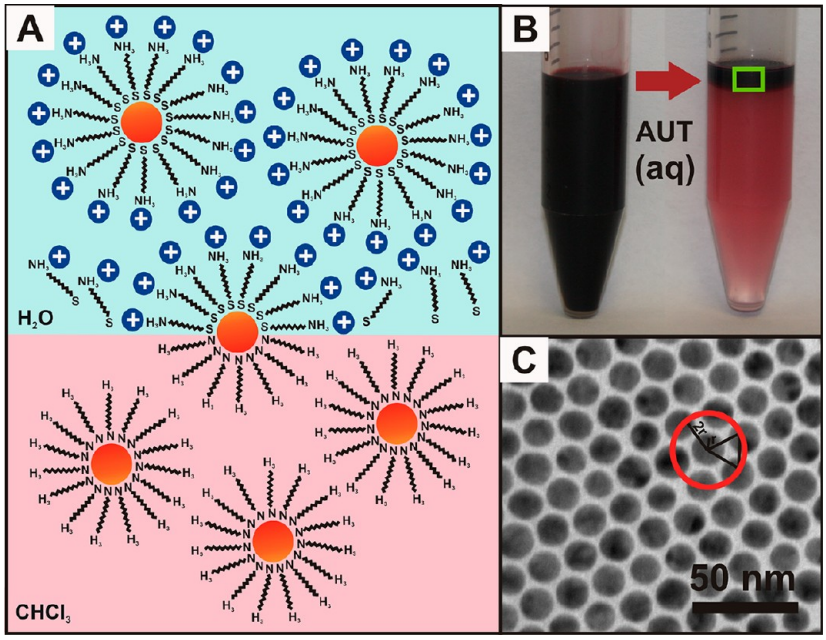

Figure 1. (A) Schematic representation of the phase-transfer mechanism for the preparation of cationic Au NPs (not drawn to scale). (B) View of highly concentrated Au NPs (~13 nm) suspended in chloroform (left) and after phase transfer into an aqueous solution using 11-amino-1-undecanethiol (AUT) (right). (C) TEM image of the Au NPs after phase transfer with AUT.

tetraalkylammonium salts,[16,25] and amino acids[11] to Au NPs, which were then examined in a variety of therapeutic uses. A third possibility involves citrate-synthesized aqueous Au NPs, which presents the advantage of simple surface functionalization and permits the control of the core size from 8 to 150 nm by adjusting the citrate-to-gold ratio.[31] However, in this case the direct negative citrate displacement by positively charged molecules causes multiple electrostatic bridging, leading to irreversible agglomeration of the conjugates.[32−35] Therefore, only a few studies have successfully prepared cationic particles upon surface ligand exchange on citrate-synthesized Au NPs, which involved a previous removal step of sodium citrate either by displacement with thioctic acid[23] or by centrifugation.[9] Such approaches led to either mixed-ligand Au NP surfaces or unavoidable minor agglomeration effects, respectively.

When rethinking ways to obtain cationic NPs in biological environments, it is worth mentioning that, in contrast to aqueous protocols, organic synthetic methods usually produce higher quality nanocrystals with narrower dispersions and at high concentrations due to the highly efficient steric stabilization. In this work, we have successfully prepared high concentrations (*i.e.*, up to 3−4 mM of 13 nm NPs) of both cationic and anionic Au NPs in aqueous solution by means of a phase-transfer methodology employing a variety of nanocrystal sizes (4, 9, and 13 nm) with narrow size distributions (Figure 1). The key was to use intermediate transfer agents and solvents in a precise sequence. We first employed 11-amino-1-undecanethiol as a case model ligand to optimize the synthetic procedure, which was then successfully applied for the conjugation of two identical peptidic biomolecules terminating in either positive (NH_3^+) or negative (COO^-) charged groups. Our size of choice was 13 nm Au NPs, as this is the typical size of particles normally used for delivery and cellular uptake,[36−38] probably based on the fact that large NPs can easily accommodate an increased and combined biological load while still being able to penetrate and cross cell membranes. The effect of the surface charge of these Au NP-bioconjugates was finally investigated in the cellular uptake and intracellular localization on human fibroblasts (1BR3G).

RESULTS AND DISCUSSION

Preparation and Characterization of NPs. A range of different sizes of Au NPs (4, 9, and 13 nm) were initially synthesized in toluene as solvent in the presence of alkylamine surfactants. The choice of these particle sizes was based on size-dependence studies reported in the literature,[39] where phase transfer was 100% successful for ~4 nm Au NPs, but ~13 nm Au NPs did not transfer at all. In the case of Au NPs of 4 nm, the synthesis was carried out following the Brust−Schiffrin protocol by $NaBH_4$ reduction in the presence of dodecylamine,[26] while 9 and 13 nm Au NPs were prepared using oleylamine as both the reducer and surfactant simultaneously.[40] Alternatively, Au NPs of 4 nm were also first synthesized in the aqueous phase upon $NaBH_4$ reduction in the presence of sodium citrate and then transferred into toluene using an amphiphilic ligand such as tetraoctylammonium bromide (TOAB). All the syntheses resulted in

TABLE 1. UV–Vis Wavelength of Absorption Maximum, Number Size by DLS, and ζ-Potential Values of Au NPs Transferred from Chloroform (before) into Aqueous Phase (after) with AUT and Peptidic Biomolecules CIPGNVG-PEG-NH_2 and CIPGNVG-PEG-COOH

		λ_{max} (nm)		hydrodynamic diameter in nm (PDI)		ζ-potential in mV (std dev in mV)
sample	ligand	before	after	before	after	after
Au NP (4 nm)		521.0	521.0	9.2 (0.2)	7.6 (0.5)	+43.0 (10.0)
Au NP (4 nm) aqueous	AUT	525.5	522.0	14.5 (0.5)	10.9 (0.5)	+23.6 (13.0)
Au NP (9 nm)		523.0	520.0	9.8 (0.2)	11.9 (0.8)	+45.6 (8.4)
	AUT		519.0		14.1 (0.5)	+24.3 (8.4)
Au NP (13 nm)	CIPGNVG-PEG-NH_2	523.0	520.0	11.1 (0.2)	14.5 (0.3)	+10.0 (8.4)
	CIPGNVG-PEG-COOH		520.0		16.1 (0.3)	−41.5 (5.6)

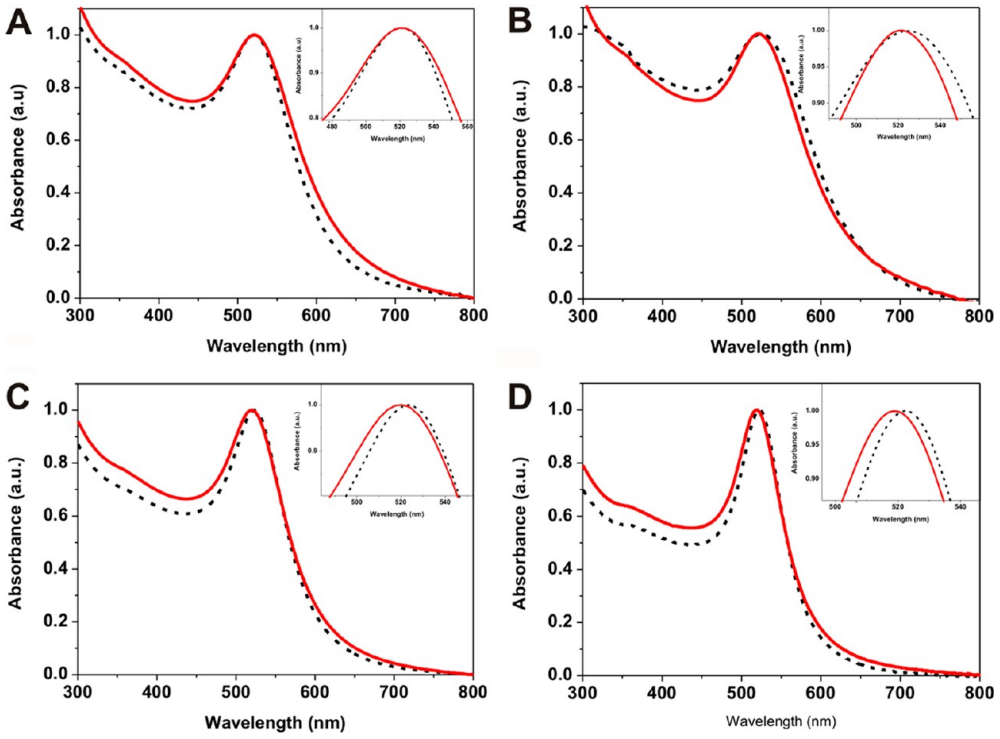

Figure 2. Normalized UV–vis absorption spectra of Au NPs before (dashed black line) and after phase transfer with AUT ligand (red line) employing different types of as-synthesized Au NPs: (A) dodecylamine-capped Au NPs (4.6 ± 1.1 nm) in toluene, (B) TOAB-Au NPs (4.9 ± 1.7 nm) in toluene after phase transfer from aqueous solvent, and oleylamine-capped Au NPs of (C) 8.9 ± 1.7 nm and (D) 13.4 ± 1.6 nm, both in toluene.

monodispersed and good-quality starting materials as observed by TEM, UV–vis spectroscopy, and dynamic light scattering (DLS) (Table 1 and Supporting Information, Figures S1, S2, and S3). After a proper elimination of excess reagents remaining from the syntheses by centrifugation, and subsequent redispersion of the particles into more polar solvents such as chloroform, surface functionalization was performed by a ligand-exchange procedure. Procedures that allow the transfer of Au NPs from organic to aqueous solvents have recently attracted much attention,[41,42] which typically involve the synthesis and stabilization of the nanocrystals in the presence of an alkanethiol. As an alternative to this, the current study deals in the first step with the use of an alkylamine as both a weaker reducer for Au^{3+}-precursor and a weak binding surfactant, so that NPs are produced under mild conditions. The subsequent replacement at the interphase of alkylamine surfactants by aqueous-soluble thiol-containing ligands that render hydrophilicity to the final NP-conjugate facilitates the transfer into the aqueous phase. This methodology overcomes the difficulties encountered in place-exchange reactions with alkanethiolate monolayers (R_1S *vs* R_2S), in which the rate and equilibrium stoichiometry are controlled by the mole ratio of R_2SH to R_1S units, their relative steric bulk, and R_1 *vs* R_2 chain lengths.[30]

Functionalization with AUT. Initial studies were carried out with 11-amino-1-undecanethiol (AUT), an aminealkanethiol with a positive charge at neutral pH. As

shown in Figure 1B, Au NPs of ~13 nm in diameter could be successfully transferred from chloroform into water using AUT at neutral pH, which led to 15-fold concentrated samples. TEM analysis of the cationic AUT-functionalized Au NPs of different sizes in water showed similarity in particle size and size distribution in comparison to as-synthesized NPs (data not shown), together with no sign of agglomeration. Surface functionalization of the Au NPs with AUT could be followed by variations of the surface plasmon resonance (SPR) peak in the UV−vis spectra (Figure 2 and Table 1), whose absence of broadening further confirmed the stability of NPs after the phase-transfer process. In most of the cases, a blue-shift of about ~3 nm of the SPR peak was observed after phase transfer, which is indicative of a modification of the surface environment of the NP, probably as a consequence of a replacement of capping ligands. Only in the case of 4 nm Au NPs synthesized in toluene could no significant variation of the SPR absorption peak be observed. Hydrodynamic diameter measurements by DLS indicated a slight variation of ~2−4 nm in diameter in all cases, which due to the different nature of the solvents and the subsequent double layer formed was unable to corroborate the exchange of ligands. However, the positive surface charge of the conjugates (between +23.6 and +45.6 mV) confirmed the new cationic coating of the particles. The efficiency of the phase transfer was evaluated by employing different concentrations of AUT both under a 0.5 molar defect over the estimated NPs' complete coverage and also under 1-, 5-, and 10-fold molar excess of AUT (Figure 3A). In all cases the Au NPs transferred well, but a defect in the ligand made the NPs immediately agglomerate in the aqueous phase, as observed in the UV−vis absorbance spectra, probably due to the poor stabilization of the NP surface caused by the incomplete coating of the surface. A successful phase transfer to the aqueous layer was also obtained from Au NPs (~13 nm) dispersed in a set of different organic solvents (toluene, DCM, and THF) (Figure 3B).

Functionalization with Peptidic Biomolecules. Peptides were chosen as archetypical ligands because of their chemical properties analogous to those of proteins, their versatile chemistry, which provides the functional groups found in the 20 natural amino acids, and their ability to form self-assembled monolayers at the surface of nanomaterials.[43] In our previous studies, biomolecules based on the peptide sequence (CIPGNVG) with two different C-terminal PEG moieties, ending in either amine ($-NH_2$) or acidic (−COOH) functional groups, were tested.[34] The choice of these types of biomolecules was based on their interest in cosmetics to stimulate collagen production. We decided to employ the same ligands as a proof-of-concept of the phase-transfer methodology developed in the present work and to provide robust and scalable

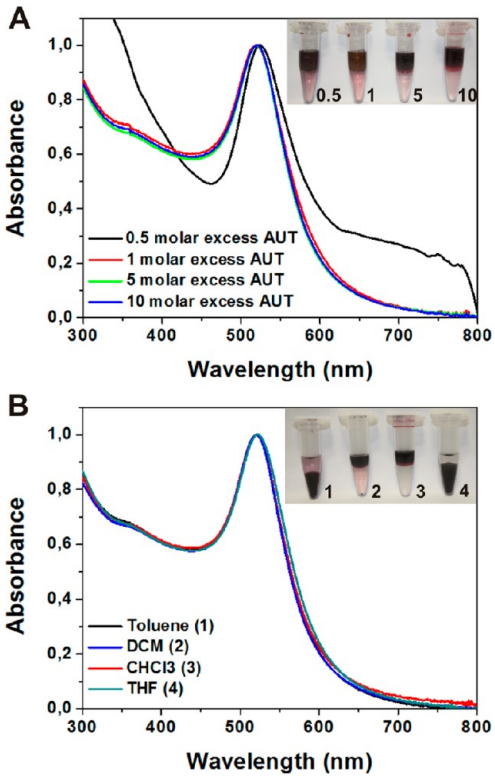

Figure 3. (A) Normalized UV−vis absorption spectra of Au NPs (~13 nm) after phase transfer from chloroform into water and surface functionalization using a 0.5-, 1-, 5-, and 10-fold molar excess of AUT. (Inset) Images showing the phase-transferred NPs. (B) Normalized UV−vis absorption spectra of Au NPs (~13 nm) after phase transfer from a variety of solvents and surface functionalization using 50-fold molar excess of AUT. (Inset) Images showing the phase-transferred NPs.

methodologies for preparing cationic Au NPs. The design of the peptide sequence took into account the need to have a strong affinity for Au surfaces *via* Cys residues, the ability to self-assemble into a dense layer that excludes water due to the hydrophobic residues, and a hydrophilic PEG terminus to ensure high solubility in water. Under the same reaction conditions as with the AUT ligand, oleylamine-stabilized Au NPs (~13 nm in diameter) could be transferred from chloroform into water using a 50-fold molar excess of peptidic biomolecules CIPGNVG-PEG-NH_2 or CIPGNVG-PEG-COOH. As in the case of AUT, the UV−vis spectrum of Au NPs after phase transfer and surface functionalization showed a blue-shift of the SPR peak (3 nm) for both negative and positive peptidic bioconjugates (Table 1). Hydrodynamic diameter measurements by DLS indicated an increase of ~3−5 nm in diameter in both cases, with respect to the volume size of oleylamine-stabilized Au NPs. ζ-Potential measurements at neutral pH = 7.5 confirmed either the cationic or the anionic nature of bioconjugates Au NP-CIPGNVG-PEG-NH_3^+ (+10.0 mV) and Au NP-CIPGNVG-PEG-COO^- (−41.5 mV), respectively,

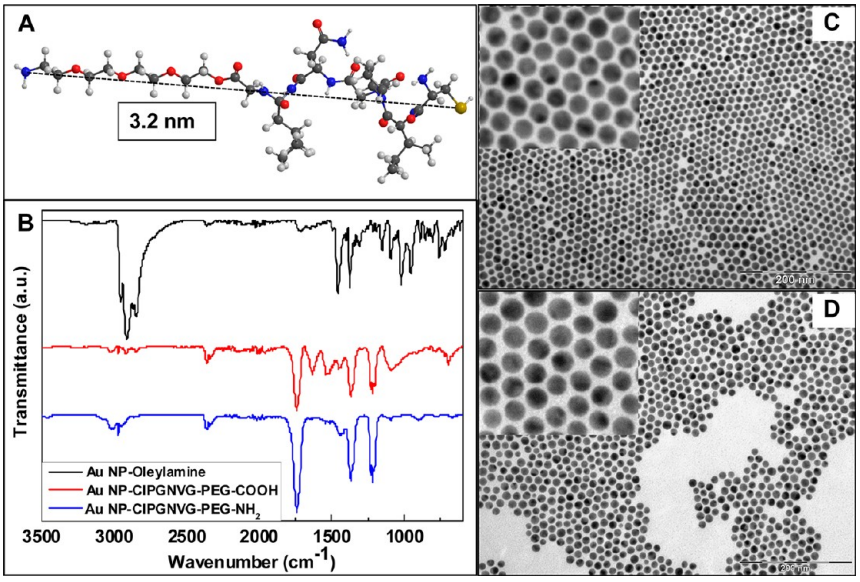

Figure 4. (A) Minimum energy structure geometry of peptidic biomolecule CIPGNVG-PEG-NH_2 calculated using ChemBio-Draw 3D. (B) FTIR spectra of oleylamine-capped Au NPs before (black) and after the ligand-exchange reaction with CIPGNVG-PEG-COOH (red) and CIPGNVG-PEG-NH_2 biomolecules (blue). Representative TEM images of Au NPs (~13 nm) functionalized with peptidic biomolecules CIPGNVG-PEG-NH_2 (C) and CIPGNVG-PEG-COOH (D) after the phase transfer from chloroform into the aqueous phase.

whose absolute values indicated a dense packing of the ligands on the surface of the particles.

The successful refunctionalization of Au NPs after the phase-transfer process was confirmed by FTIR spectroscopy (Figure 4B). After the ligand-exchange reaction, the band at 2912 cm^{-1} corresponding to the C–H stretching mode next to the double bond of oleylamine capping molecules is clearly eliminated. In the meantime, the band at 1740 cm^{-1} corresponding to the amide groups of the peptidic sequences is detectable after the exchange reaction. Furthermore, the spectral change in the 1450–1680 cm^{-1} region seems to support the presence of bands corresponding to the symmetric and asymmetric stretching modes in the carboxylate group of the peptidic biomolecule CIPGNVG-PEG-COOH. It should be noted that the peptidic-capped Au NPs could be lyophilized and stored as a powder for further utilization, and when redissolved in water, they display exactly the same UV–vis absorption spectrum as before freeze-drying. This is important since only a few nanobioconjugate preparations can be stored in the dry state and then redispersed in water without irreversible agglomeration.[33] Analysis by TEM showed the formation of self-assembled monolayers of Au NPs, which is indicative of the high solubility and mobility of the particles in solution (Figure 4C, D).[44] The ordered arrangements of Au NPs have an interparticle spacing of approximately 2–3 nm, which is slightly below the limit of what would be expected for 2 times the size of these biomolecules (~3.2 nm in a stretched form, Figure 4A). Such an observation could be an effect of the drying process of the samples on TEM grids and the subsequent packing of the biomolecules.

Internalization Studies of Peptidic Bioconjugates. To study the effect of the surface charge of Au NPs on the interaction with biological systems, the two peptidic biomolecules CIPGNVG-PEG-NH_2 and CIPGNVG-PEG-COOH, with identical core structures but differing only in the functional end groups that give the net surface charge at neutral pH, were chosen. The interaction of NPs with the extracellular matrix results in the formation of a bioshell also known as a protein corona, which accompanies the NP, confers biological identity, and hardens with time (from transient to permanent).[10,45] The stability of the bioconjugates was tested first after incubation in borate buffer solution (2 mM, pH 8.5) containing 10% FBS followed by dilution in cell culture medium (CCM). No formation of agglomerates could be observed after 24 h (Supporting Information, Figure S4). The CCM used contained 10% FBS, which is a multicomponent fluid containing up to 1.8 mg/mL of glucose and 70 mg/mL of proteins, among which albumin is the most abundant (~51% of total protein content) followed by globulins (~24% of total protein content) and hemoglobin (<0.3% of total protein content). UV–vis absorption spectroscopy allowed easy monitoring of the interaction of both bioconjugates Au NP-CIPGNVG-PEG-NH_3^+ and Au NP-CIPGNVG-PEG-COO^- with serum proteins, since the SPR is highly sensitive to the NP environment and agglomeration (Supporting Information, Figure S5 and Table S1). In the case of anionic Au NP-bioconjugates, identical peaks are observed in the CCM. Note that proteins are

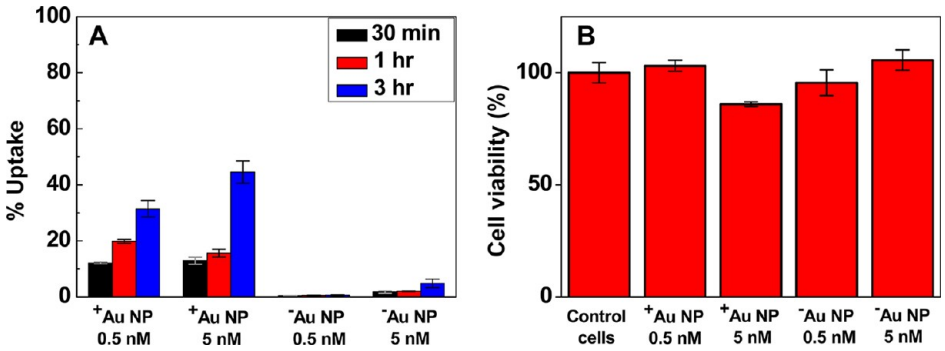

Figure 5. (A) Intracellular Au concentration as determined by ICP-MS as a function of time and (B) XTT cell viability test after 24 h, both upon incubation of Au NP-ClPGNVG-PEG-NH_3^+ and Au NP-ClPGNVG-PEG-COO^- bioconjugates in human fibroblast (1BR3G) cells. Data represent the average of three replicate wells with standard deviation.

normally anionic, like these NPs, so the interaction is weak. For the cationic bioconjugates, a peak shift is observed, indicating a stronger NP−protein interaction. In CCM one can observe a certain broadening of the peak, which can be attributed to the purification step when many cationic NPs share few anionic proteins from the rest of the serum during the rinsing phases, thus resulting in a certain degree of agglomeration. Regarding surface charge, starting from different points, an evolution toward the surface charge of the medium as time passes is observed for both cationic and anionic bioconjugates. In these experiments, the NPs are purified after a certain incubation time, and the remaining protein irreversibly associated with the particle surface is correlated with the size and surface state of the NP−protein complex.[10,45] Finally, both incubated bioconjugates with only DMEM lead to agglomeration after 5 h, which is due to the screening of the electrostatic repulsion between the charged terminus of the peptidic chains and is in agreement with our previous studies of bioconjugate stability as a function of the ionic strength.[34] This result confirms the presence of loosely bound proteins in the case of anionic Au NP-bioconjugates, which are responsible for the observed stability in CCM.

The intracellular uptake of the bioconjugates was then tested *in vitro* with human fibroblasts. 1BR3G cells were incubated for 30 min, 1 h, and 3 h with two different concentrations (0.5 and 5 nM NPs, corresponding to approximately 5 and 50 μg of Au, respectively) of either Au NP-ClPGNVG-PEG-NH_3^+ or Au NP-ClPGNVG-PEG-COO^- in serum-containing medium. After centrifugation the Au content of both the medium of the cells after a certain incubation time and the pellets from the trypsinized cells was determined by ICP-MS. As anticipated from the higher affinity of cationic molecules for cell membranes, significantly all the cases showed a higher uptake of the cationic bioconjugates when compared with their anionic counterparts (Figure 5A). The highest uptake (44.5%) could be observed for 5 nM cationic Au NP-bioconjugates after 3 h, and a 10-fold dilution of the particles resulted in 31.5% of uptake during the same incubation time. This contrasts with the maximum 5% of uptake observed in the best case of internalization with anionic Au NP-bioconjugates (incubation of 3 h at 5 nM NP concentration). We assume that this technique may not distinguish between the internalized Au NPs and those attached on the outside of cell membranes. However, Au NPs have been recurrently seen to be endocytosed after interacting with the membrane of cells in a process of a few hours.[36,46] Under this assumption the estimated number of internalized/adsorbed cationic Au NP-bioconjugates was 9.1×10^7 per cell,[47] which is much higher than other reported values (approximately 2.0×10^5 NPs per cell for 15.5 nm Au NPs) using similar methods.[48]

Cell viability on human fibroblast 1BR3G cells was evaluated using the well-established XTT assay, which measures the respiratory activity of the cells (Figure 5B). Importantly, after 24 h of incubation with both positive and negative Au NP-bioconjugates none of the particles showed a significant toxicity at concentrations of 0.5 and 5 nM of NPs. This result is significant given the high extent of cellular uptake in the case of cationic Au NP-bioconjugates. Further toxicity assessment was also performed by a standard Trypan blue exclusion assay carried out after both 3 and 24 h of incubation with positive and negative Au NP-bioconjugates at 5 nM NPs (Figure 6). Comparative optical microscope images indicated that cells were alive, as indicated by the absence of blue color. In addition, optical microscope images after incubation of Au NP-bioconjugates showed no sign of toxicity, as the morphology of the cells was maintained and no major detachment occurred (Supporting Information, Figure S6). Overall, there was no indication of any effects the particles might have on cell metabolism or proliferation in the fibroblast 1BR3G cells tested. However, we are well aware that the cell type can have quite a significant role in the definition of suitable pathways for detoxification of NPs, which has deep implications for biomedical applications.[49,50]

Confocal fluorescence microscopy was used to confirm and assess the enhanced uptake of NPs in

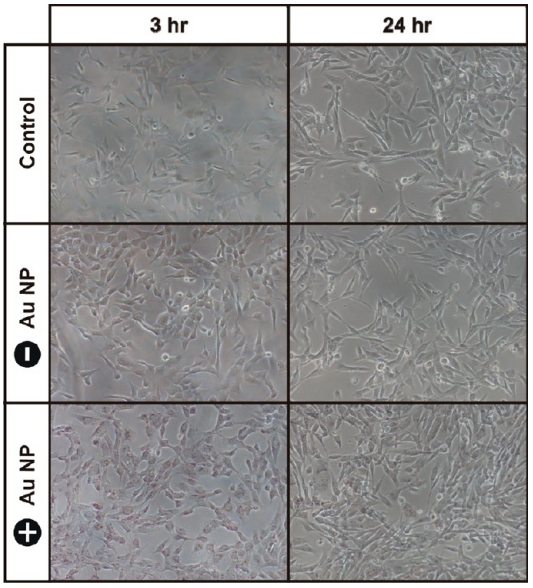

Figure 6. Toxicity of Au NP-ClPGNVG-PEG-NH_3^+ and Au NP-ClPGNVG-PEG-COO^- bioconjugates at 5 nM NPs in human fibroblast (1BR3G) cells as determined by the Trypan blue test and analyzed by comparative optical microscope images. Blue color represents dead cells.

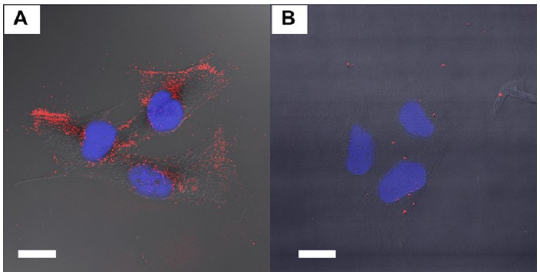

Figure 7. Confocal images of human fibroblast (1BR3G) cells incubated with Au NP-ClPGNVG-PEG-NH_3^+ (A) and Au NP-ClPGNVG-PEG-COO^- (B) bioconjugates at 5 nM NP concentrations for 3 h. Nuclei were stained with DAPI, showing blue fluorescence. The scattering from Au NPs is false-colored in red. Slides of 0.25 μm of the confocal fluorescence, reflectance, and differential interference contrast transmission images were obtained independently and then overlaid in a maximal projection mode. The scale bars are ~20 μm.

living cells. This technique is normally used to track fluorescently labeled molecules, but here the Au NPs were visualized by the light reflected when irradiated with a laser at 488 nm. While fibroblast cells incubated with Au NP-ClPGNVG-PEG-COO^- (Figure 7B) presented low-reflection signals, those incubated with Au NP-ClPGNVG-PEG-NH_3^+ (Figure 7A) showed increased reflected light both interacting with the cell membrane and accumulated in the cytoplasm. After optical sectioning (slides of 0.25 μm) and spatial reconstruction of cells, confocal microscopy allowed the observation of cationic Au NP-bioconjugates homogeneously distributed throughout the cytoplasm (Supporting Information, movies 1 and 2). However, from the reconstructions it was difficult to confirm nuclear localization

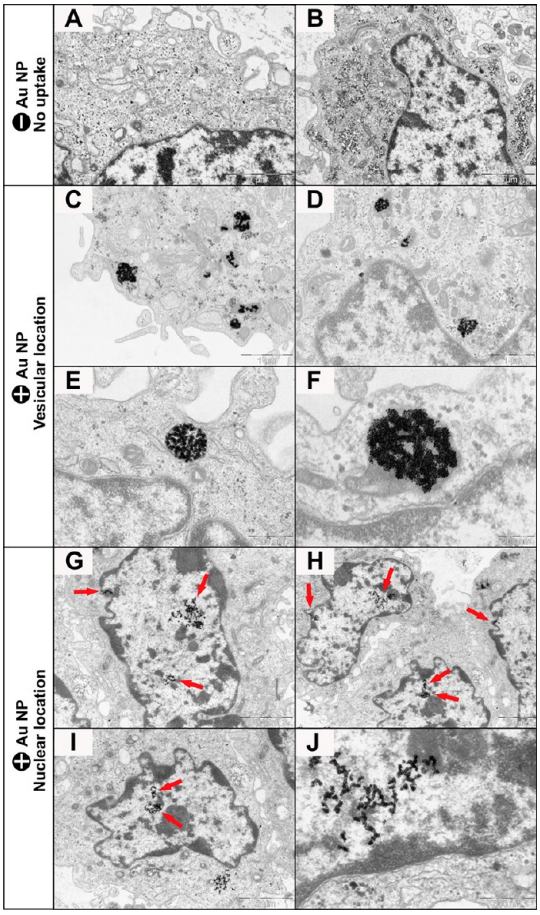

Figure 8. TEM images of human fibroblast (1BR3G) cells incubated with Au NP-ClPGNVG-PEG-COO^- (A, B) and Au NP-ClPGNVG-PEG-NH_3^+ (C–J) bioconjugates at 5 nM NP concentrations for 3 h. (A, B) Cells incubated with Au NP-ClPGNVG-PEG-COO^- showing no NP uptake, (C–F) cells incubated with Au NP-ClPGNVG-PEG-NH_3^+ showing NPs confined to endocytic vesicles, and (G–J) cells incubated with Au NP-ClPGNVG-PEG-NH_3^+ showing the presence of NPs in the nucleus.

of the bioconjugates. In all the experiments, contrast phase and bright field were used to assess normal cell morphology and nuclei were labeled with DAPI. These results confirm that cationic Au NP-bioconjugates bind more efficiently to cell membranes and induce higher levels of cellular uptake.

TEM was used as the main tool for the localization of the Au NPs inside the cells. Diffraction contrast (Supporting Information, Figure S7) was employed to unequivocally discriminate between Au NPs and the other features of the cell, according to the high electronic density and crystallinity of gold. Cationic Au NP-bioconjugates were incubated with fibroblast cells for 3 h and were then found to be confined to the endocytic vesicles as shown in Figure 8. This suggests that the predominant route of cellular uptake is endocytosis and that the cationic NPs maintain some of their cationic character and surface characteristics after interaction with the extracellular matrix, at least during the first hours of the *in vitro* experiment. It can be

argued that with time, during the interaction of the bioconjugates with the physiological medium, interaction with serum proteins, and a progressive hardening of the protein corona, agglomeration or chemical modification of the functional groups may deactivate these vectors. In our case, the positive surface charge of the Au NPs may be responsible for an increased interaction with the cell membrane, probably being attracted and attaching to it due to the intrinsic negative charge of the phospholipid bilayers. From there, it appears that NPs do not penetrate and cross the membrane but accumulate until the membrane is recycled and NPs are internalized inside endosomes, as TEM indicates. Notably, the cationic Au NP-bioconjugates within the endosomes show little stability against agglomeration, which could be either due to ligand-exchange reactions within the cell[51] or the result of the digestion of the ligand shell by proteases inside the endosome. However, a large proportion of the particles seem to migrate toward the vicinity of the nucleus, and indeed, nuclear localization of the Au NP-bioconjugates could also be observed, which suggested that the biomolecules were acting as nuclear localization signals guided by their positive charge. Apparently, inside the endosome the cationic bioconjugates are still active and may become even more positively charged in the acidic environment of the late endosomes/endolysosomes, resulting in membrane perturbation as in the case of proton sponges,[52] which would justify the break of the endosome near the nucleus and the consequent penetration of the cationic Au NPs. Experiments to determine how the particles escape from the endosomes and enter the nucleus are the subject of an ongoing study. Finally, in agreement with ICP-MS and confocal studies, no significant uptake was observed for anionic Au NP-bioconjugates.

CONCLUSIONS

In this work, the great potential and feasibility of the phase-transfer methodology has been demonstrated for different types of ligands (*i.e.*, AUT, peptidic biomolecules) to yield both anionic and cationic functionalized Au NPs. In particular, this method overcomes the agglomeration difficulties observed for conjugation of positively charged ligands in the presence of negatively charged stabilizers such as citrate. Large amounts of highly monodisperse and highly concentrated samples of cationic Au NPs have been obtained. The enhanced affinity for cell membranes and uptake of cationic bioconjugates over negative ones has been demonstrated in the case of two ligands with identical chemical core structure but just differing in the surface charge. The nuclear localization observed for the cationic Au NP-bioconjugates upholds promising applications in gene delivery, where oligonucleotides are loaded onto the particles and are carried into the cells with potentially higher efficiency than unbound DNA. Ongoing work focuses on elucidating the mechanism of endosomal escape and nuclear entry.

EXPERIMENTAL SECTION

Materials. Sodium citrate, tetraoctylammonium bromide (98%), dodecylamine (98%), oleylamine (70%), 11-amino-1-undecanethiol hydrochloride (99%), methanol anhydrous (99.9%), ethanol (90%), toluene (99.8%), chloroform (99%), dichloromethane (DCM, 99.8%), and tetrahydrofuran (THF, 99.9%) were purchased from Sigma-Aldrich and used as received without further purification. Peptidic biomolecules CIPGNVG-PEG-COOH and CIPGNVG-PEG-NH_2 (PEG = polyethyleneglycol of MW = 220) were synthesized following an Fmoc strategy and solid-phase synthesis (bioNova Científica S.L., Spain). Stock solutions (10 mM) of AUT and peptides were prepared upon dilution in either Milli-Q H_2O or in a (85:15) mixture of ethanol/Milli-Q H_2O, respectively, and the resulting solutions were filtered using 0.2 μm filters and used immediately under sterile conditions.

Characterization. UV−vis absorption spectra were recorded with a Shimadzu UV-2401PC spectrophotometer at room temperature. The samples were left to settle for 30 min before measurements. Au NPs were visualized using a transmission electron microscope, TEM (JEOL 1010, Japan), at an accelerating voltage of 80 kV. The sample (10 μL) was drop-casted onto ultrathin Formvar-coated 200-mesh copper grids (Tedpella Inc.) and left to dry in air. For each sample, the size of 200 particles was measured to obtain the average and the size distribution. Digital images were analyzed with ImageJ software and a custom macro performing smoothing (3 × 3 or 5 × 5 median filter), manual global threshold, and automatic particle analysis provided by ImageJ. The macro can be downloaded from http://code.google.com/p/psa-macro. DLS and ζ-potential measurements were obtained using a Zetasizer Nano ZS (Malvern Instruments). Standard purification by dialysis, unless otherwise stated, was performed using 16 mm membranes (MWCO = 15 kDa) against distilled H_2O (5000 mL). FTIR spectra were recorded on a Tensor27 Bruker spectrometer equipped with ATR (attenuated total reflection) from MKII Golden Gate, Specac. The samples were liophilized for FTIR measurements. Au content of the cell samples was determined by an Agilent inductively coupled plasma mass spectrometry (ICP-MS) instrument (model: 7500cx) with a detection limit of 0.02386 ppb. Both the supernatant and the pellet samples were digested in *aqua regia* at 100 °C before ICP-MS analysis. Ga was used as the internal standard, and the integration time/point and time/mass were 0.1 and 0.3 s, respectively, with a 3× repetition. The confocal images were acquired using a Leica TCS SP5 epifluorescence/reflectance laser scanning confocal microscope with a 63× oil immersion objective. The excitation was provided by an Ar multiline laser. Consistent laser intensity or camera exposure levels for each fluorescent marker in each experiment were used. Reflectance images were obtained with 488 nm laser excitation. Images were treated using Leica Microsystems LAS AF lite analysis software. Optical microscope images were acquired using an inverted Nikon TS100F optical microscope with an integrated Nikon DS-Fi2/U3 digital camera.

Synthesis of Au NPs (4 nm) in Toluene. Au NPs of ∼4 nm in diameter were prepared in toluene by a modification of the Brust−Schiffrin two-phase approach.[26] Briefly, a solution of 30 mM $HAuCl_4 \cdot 3H_2O$ was first transferred from an aqueous (30 mL) to a toluene (80 mL) solution containing TOAB (2.2 g, 50 mM), which was followed by reduction with a freshly prepared aqueous solution of $NaBH_4$ (25 mL, 0.4 M) in the

presence of dodecylamine (155.7 mg, 0.84 mmol). Particle size was determined by DLS and TEM (Supporting Information, S1A).

Synthesis of Au NPs (4 nm) in Water and Phase Transfer to Toluene. Au NPs of ~4 nm were prepared in aqueous phase by the method reported by Jana *et al.*[53] Briefly, 0.6 mL of an ice-cold and freshly prepared aqueous solution of 0.1 M $NaBH_4$ was added dropwise to 20 mL of an aqueous solution containing $HAuCl_4 \cdot 3H_2O$ (2.0 mg, 0.25 mM) and trisodium citrate (1.5 mg, 0.25 mM) under vigorous stirring. The as-synthesized Au NPs were then transferred into toluene following reported procedures,[39] by using TOAB (0.7 g, 0.13 M) as the phase-transfer reagent at a H_2O/toluene volume ratio of 1:1. Particle size was determined by DLS and TEM (Supporting Information, S1B).

Synthesis of Au NPs (9 and 13 nm) in Toluene. Au NPs of ~9 and ~13 nm in diameter were prepared in toluene in a one-pot synthesis by a reported method.[40] Briefly, a solution of $HAuCl_4 \cdot 3H_2O$ (393 mg, 1 mmol) in toluene (50 mL) was mixed with oleylamine (4.6 mL, 10 mmol), which acts as both the reducing agent and surfactant of the resulting Au NPs. The reaction mixture was kept under N_2 protection and heated to either 65 °C for 6 h or 115 °C for 3 h to obtain ~9 and ~13 nm Au NPs, respectively. Particle size was determined by DLS and TEM (Supporting Information, S1C and S1D).

Phase Transfer and Surface Functionalization of Au NPs. Methanol (3 mL) was added to a solution of as-synthesized Au NPs in toluene (5 mL), the cloudy mixture was centrifuged (3000 rcf, 5 min) to precipitate the particles, and the supernatant was discarded. The resulting pellet was resuspended in toluene (5 mL), and the complete cleaning process was repeated. The particles were finally dispersed in chloroform (5 mL). In order to ensure complete coating of the Au NPs, the phase-transfer process was carried out in the presence of an excess of ligand (calculated by the number of Au atoms at the surface of the NP and assuming that each thiolated molecule occupies 21.4 $Å^2$ of the Au NP surface).[54,55] A solution of the desired ligand in a 50-fold molar excess, either AUT diluted in water or the biomolecule CIPGNVG-PEG-NH_2 or CIPGNVG-PEG-COOH diluted in ethanol (500 μL), was added dropwise to a solution of Au NPs in chloroform (1 mL). In the case of AUT, immediate transfer was observed after gentle vortexing. However, for the peptidic biomolecules a few drops (approximately 300 μL) of 0.1 M of either HCl or NaOH were required to form the respective charged compounds, followed by some additional mixing. The biphasic mixture was left to stand on the bench for about 10–30 min, during which it could be observed how the red color of the organic solution was transferred into the aqueous layer. The resulting bioconjugates in the aqueous layer were exhaustively purified by dialysis against Milli-Q water with two cycles of 24 h each in order to eliminate the excess nonconjugating molecules. NP functionalization and stability of the bioconjugates were determined by UV–vis absorbance spectroscopy, DLS, and TEM. Similarly, experiments with different ligand molar ratios were performed under the same reaction conditions using Au NPs (~13 nm) in chloroform and a 0.5-, 1-, 5-, and 10-fold molar excess of AUT. A variety of organic solvents of different polarity (toluene, DCM, and THF) were also employed besides chloroform in the same phase-transfer protocol using Au NPs (~13 nm) and a 50-fold molar excess of AUT.

Cell Culture and Particle Incubation. Human fibroblasts (1BR3G, ECACC/Sigma-Aldrich) were cultured in Dulbecco's modified Eagle's medium (DMEM) supplemented with 10% fetal bovine serum (FBS) under a humidified 10% CO_2 atmosphere at 37 °C. For Au NP uptake studies cells were seeded at a density of 10^5 cells per well in six-well plates. After 48 h cells were washed with PBS, and fresh culture medium (1 mL) was added containing the functionalized Au NP-bioconjugates. Previously to the incubation with cells, both conjugates Au NP-CIPGNVG-PEG-NH_2 and Au NP-CIPGNVG-PEG-COOH at a concentration of 50 nM of NPs were irradiated with UV light for 1–2 h, incubated overnight (1:2 dilution) in borate buffer solution (2 mM, pH 8.5) containing 10% FBS, and diluted in DMEM 10% FBS medium up to final concentrations of 0.5 and 5 nM of NPs. All samples were centrifuged (8000 rcf, 10 min) and resuspended in Milli-Q H_2O before UV–vis, DLS, and ζ-potential measurements were performed to test the stability of the conjugates. After a certain incubation time (30 min, 1 h, and 3 h), the medium of the cells was collected for ICP-MS analysis, and the cells were washed three times with PBS (1 mL), trypsinized (Trypsin-EDTA, 1 mL), and centrifuged (400 rcf, 10 min). The resulting pellets were also collected for ICP-MS analysis. The percentage of cell-associated particles was calculated relative to the total number of particles used in the incubation medium and compared well with the decrease of particles observed in the incubation medium after cell exposure in all the cases.

For confocal studies cells were seeded at a density of 5×10^4 cells per well on glass coverslips placed in six-well plates and cultured at 37 °C and 10% CO_2 in an incubator. After 48 h, cells were washed with PBS, and fresh medium was added containing 5 nM of the functionalized Au NP-bioconjugates. After 3 h of incubation, cells were washed three times with PBS (1 mL) and fixed in ice-cold methanol (1 mL) for 15 min at −20 °C. Methanol was then allowed to evaporate before cells were washed three times with PBS/0.005% Tween 20 (1 mL), and the nuclei were stained with DAPI for 15 min. Glass coverslips were mounted on a slide with Fluoprep mounting medium (Biomerieux).

For toxicity determination 5×10^3 cells per well were seeded in 96-well plates and incubated overnight to allow for cell attachment. After overnight incubation, cells were washed with PBS and fresh culture medium (100 μL) was added containing the Au NP-bioconjugates at the desired concentration and incubated for 24 h. Although the duplication time for the 1BR3G cells is approximately 20 h, the cells did not reach confluency at the end of the assay. The concurrent cell viability assay was performed using the XTT assay (Biomedica) in 96-well plates according to the manufacturer's instructions. In brief, XTT reagent (20 μL) was added to the cell culture and incubated for 2 h. After incubation the absorbance was recorded at 450 nm (reference wavelength 620 nm) in a microplate reader (Victor 3, PerkinElmer). All conditions were performed in quadruplicate. Cell viability was additionally determined by a Trypan blue dye exclusion assay. After 24 h exposure to Au NP-bioconjugates, the cells were rinsed with fresh medium in order to eliminate excess Au NPs and 0.4% Trypan blue solution was added and left for 3 min. The cells were then rinsed thoroughly with PBS buffer and inspected under a phase contrast microscope.

For resin inclusion for TEM, cells were thoroughly washed with PBS buffer after incubation and fixed in a 0.1 M PB solution containing 2.5% glutaraldehyde at 4 °C for 1 h. The cells were then rinsed three times with PBS and carefully collected in a tube with a cell scraper. The cellular pellet was postfixed in 1% osmium tetroxide solution for 1 h, rinsed with PBS and distilled water, and dehydrated in a graded series of ethanol (30, 60, 70, 80, and 100%). Finally warm epoxy resin was mixed with ethanol (1:1) for infiltration, and only resin was used for cell embedding (60 °C, 48 h). Ultrathin sections (50 nm) were cut with a Leica Ultracut UCT Ultramicrotome and stained with 5% uranyl acetate in 50% ethanol and 2% aqueous lead citrate solution. The sections obtained were imaged using a TEM (JEOL 1010, Japan) at an accelerating voltage of 80 kV.

Conflict of Interest: The authors declare no competing financial interest.

Acknowledgment. The authors thank Aleix Conesa and Beatriz Guerrero from Leitat Technological Center for ICP-MS analyses, Mónica Roldán and Martí de Cabo from Servei de Microscopia (UAB), and Juan Luís Monteagudo from Leica Microsystems Spain for help in confocal measurements, Nieves Hernández and Carmen López-Iglesias from Centres Científics i Tecnològics de la Universitat de Barcelona (CCiTUB) for their help in cellular processing for TEM and scientific discussion, and Laura Boix from Programa Joves i Ciència de CatalunyaCaixa for help in the synthesis of Au NPs. This work was supported by grants from the Spanish Ministry of Science and Innovation (MAT2009-14734-C02-01 and BIO2010-22321-C02-01).

Supporting Information Available: TEM images of as-synthesized Au NPs in organic solvents, DLS and ζ-potential of Au NPs transferred into aqueous phase, images, TEM micrographs, UV–vis absorption spectra, DLS and ζ-potential measurements of bioconjugates Au NP-CIPGNVG-PEG-NH_3^+ and Au NP-CIPGNVG-PEG-COO^- after incubation in CCM, and optical microscope as well as TEM images of 1BR3G cells incubated with

bioconjugates. This information is available free of charge *via* the Internet at http://pubs.acs.org.

REFERENCES AND NOTES

1. Alivisatos, A. P. Less is More in Medicine. *Sci. Am.* **2001**, *285*, 66–73.
2. Niemeyer, C. M. Nanoparticles, Proteins, and Nucleic Acids: Biotechnology Meets Materials Science. *Angew. Chem., Int. Ed.* **2001**, *40*, 4128–4158.
3. Sperling, R. A.; Rivera Gil, P.; Zhang, F.; Zanella, M.; Parak, W. J. Biological Applications of Gold Nanoparticles. *Chem. Soc. Rev.* **2008**, *37*, 1896–1908.
4. Chithrani, B. D.; Ghazani, A. A.; Chan, W. C. W. Determining the Size and Shape Dependence of Gold Nanoparticle Uptake into Mammalian Cells. *Nano Lett.* **2006**, *6*, 662–668.
5. Boisselier, E.; Astruc, D. Gold Nanoparticles in Nanomedicine: Preparations, Imaging, Diagnostics, Therapies and Toxicity. *Chem. Soc. Rev.* **2009**, *38*, 1759–1782.
6. Verma, A.; Stellacci, F. Effect of Surface Properties on Nanoparticle−Cell Interactions. *Small* **2010**, *6*, 12–21.
7. Cho, E. C.; Xie, J.; Wurm, P. A.; Xia, Y. Understanding the Role of Surface Charges in Cellular Adsorption *versus* Internalization by Selectively Removing Gold Nanoparticles on the Cell Surface with a I2/KI Etchant. *Nano Lett.* **2009**, *9*, 1080–1084.
8. Arvizo, R. R.; Miranda, O. R.; Thompson, M. A.; Pabelick, C. M.; Bhattacharya, R.; Robertson, J. D.; Rotello, V. M.; Prakash, Y. S.; Mukherjee, P. Effect of Nanoparticle Surface Charge at the Plasma Membrane and Beyond. *Nano Lett.* **2010**, *10*, 2543–2548.
9. Harush-Frenkel, O.; Debotton, N.; Benita, S.; Altschuler, Y. Targeting of Nanoparticles to the Clathrin-Mediated Endocytic Pathway. *Biochem. Biophys. Res. Commun.* **2007**, *353*, 26–32.
10. Casals, E.; Pfaller, T.; Duschl, A.; Oostingh, G. J.; Puntes, V. Time Evolution of the Nanoparticle Protein Corona. *ACS Nano* **2010**, *4*, 3623–3632.
11. Ghosh, P. S.; Kim, C.-K.; Han, G.; Forbes, N. S.; Rotello, V. M. Efficient Gene Delivery Vectors by Tuning the Surface Charge Density of Amino Acid-Functionalized Gold Nanoparticles. *ACS Nano* **2008**, *2*, 2213–2218.
12. Li, P.; Li, D.; Zhang, L.; Li, G.; Wang, E. Cationic Lipid Bilayer Coated Gold Nanoparticles-Mediated Transfection of Mammalian Cells. *Biomaterials* **2008**, *29*, 3617–3624.
13. Niidome, T.; Nakashima, K.; Takahashi, H.; Niidome, Y. Preparation of Primary Amine-Modified Gold Nanoparticles and Their Transfection Ability into Cultivated Cells. *Chem. Commun.* **2004**, 1978–1979.
14. Sandhu, K. K.; McIntosh, C. M.; Simard, J. M.; Smith, S. W.; Rotello, V. M. Gold Nanoparticle-Mediated Transfection of Mammalian Cells. *Bioconjugate Chem.* **2002**, *13*, 3–6.
15. Railsback, J. G.; Singh, A.; Pearce, R. C.; McKnight, T. E.; Collazo, R.; Sitar, Z.; Yingling, Y. G.; Melechko, A. V. Weakly Charged Cationic Nanoparticles Induce DNA Bending and Strand Separation. *Adv. Mater.* **2012**, *24*, 4261–4265.
16. Kim, B.; Han, G.; Toley, B. J.; Kim, C.-k.; Rotello, V. M.; Forbes, N. S. Tuning Payload Delivery in Tumour Cylindroids Using Gold Nanoparticles. *Nat. Nanotechnol.* **2010**, *5*, 465–472.
17. Kim, C.; Agasti, S. S.; Zhu, Z.; Isaacs, L.; Rotello, V. M. Recognition-Mediated Activation of Therapeutic Gold Nanoparticles Inside Living Cells. *Nat. Chem.* **2010**, *2*, 962–966.
18. Geidel, C.; Schmachtel, S.; Riedinger, A.; Pfeiffer, C.; Müllen, K.; Klapper, M.; Parak, W. J. A General Synthetic Approach for Obtaining Cationic and Anionic Inorganic Nanoparticles *via* Encapsulation in Amphiphilic Copolymers. *Small* **2011**, *7*, 2929–2934.
19. Zhang, L.; Sun, X.; Song, Y.; Jiang, X.; Dong, S.; Wang, E. Didodecyldimethylammonium Bromide Lipid Bilayer-Protected Gold Nanoparticles: Synthesis, Characterization, and Self-Assembly. *Langmuir* **2006**, *22*, 2838–2843.
20. Thomas, M.; Klibanov, A. M. Conjugation to Gold Nanoparticles Enhances Polyethylenimine's Transfer of Plasmid DNA into Mammalian Cells. *Proc. Natl. Acad. Sci.* **2003**, *100*, 9138–9143.
21. Chen, G.; Takezawa, M.; Kawazoe, N.; Tateishi, T. Preparation of Cationic Gold Nanoparticles for Gene Delivery. *Open Biotechnol. J.* **2008**, *2*, 152–156.
22. Leroueil, P. R.; Berry, S. A.; Duthie, K.; Han, G.; Rotello, V. M.; McNerny, D. Q.; Baker, J. R.; Orr, B. G.; Banaszak Holl, M. M. Wide Varieties of Cationic Nanoparticles Induce Defects in Supported Lipid Bilayers. *Nano Lett.* **2008**, *8*, 420–424.
23. Lin, S.-Y.; Tsai, Y.-T.; Chen, C.-C.; Lin, C.-M.; Chen, C.-h. Two-Step Functionalization of Neutral and Positively Charged Thiols onto Citrate-Stabilized Au Nanoparticles. *J. Phys. Chem. B* **2004**, *108*, 2134–2139.
24. Kalsin, A. M.; Kowalczyk, B.; Wesson, P.; Paszewski, M.; Grzybowski, B. A. Studying the Thermodynamics of Surface Reactions on Nanoparticles by Electrostatic Titrations. *J. Am. Chem. Soc.* **2007**, *129*, 6664–6665.
25. McIntosh, C. M.; Esposito, E. A.; Boal, A. K.; Simard, J. M.; Martin, C. T.; Rotello, V. M. Inhibition of DNA Transcription Using Cationic Mixed Monolayer Protected Gold Clusters. *J. Am. Chem. Soc.* **2001**, *123*, 7626–7629.
26. Brust, M.; Walker, M.; Bethell, D.; Schiffrin, D. J.; Whyman, R. Synthesis of Thiol-Derivatised Gold Nanoparticles in a Two-Phase Liquid-Liquid System. *J. Chem. Soc., Chem. Commun.* **1994**, 801.
27. Hostetler, M. J.; Wingate, J. E.; Zhong, C.-J.; Harris, J. E.; Vachet, R. W.; Clark, M. R.; Londono, J. D.; Green, S. J.; Stokes, J. J.; Wignall, G. D.; *et al*. Alkanethiolate Gold Cluster Molecules with Core Diameters from 1.5 to 5.2 nm: Core and Monolayer Properties as a Function of Core Size. *Langmuir* **1998**, *14*, 17–30.
28. Terrill, R. H.; Postlethwaite, T. A.; Chen, C.-h.; Poon, C.-D.; Terzis, A.; Chen, A.; Hutchison, J. E.; Clark, M. R.; Wignall, G. Monolayers in Three Dimensions: NMR, SAXS, Thermal, and Electron Hopping Studies of Alkanethiol Stabilized Gold Clusters. *J. Am. Chem. Soc.* **1995**, *117*, 12537–12548.
29. Hostetler, M. J.; Templeton, A. C.; Murray, R. W. Dynamics of Place-Exchange Reactions on Monolayer-Protected Gold Cluster Molecules. *Langmuir* **1999**, *15*, 3782–3789.
30. Templeton, A. C.; Wuelfing, W. P.; Murray, R. W. Monolayer-Protected Cluster Molecules. *Acc. Chem. Res.* **2000**, *33*, 27–36.
31. Frens, G. Controlled Nucleation For Regulation of Particle-Size in Monodisperse Gold Suspensions. *Nat.-Phys. Sci.* **1973**, *241*, 20–22.
32. Bellino, M. G.; Calvo, E. J.; Gordillo, G. Adsorption Kinetics of Charged Thiols on Gold Nanoparticles. *Phys. Chem. Chem. Phys.* **2004**, *6*, 424–428.
33. Levy, R.; Thanh, N. T. K.; Doty, R. C.; Hussain, I.; Nichols, R. J.; Schiffrin, D. J.; Brust, M.; Fernig, D. G. Rational and Combinatorial Design of Peptide Capping Ligands for Gold Nanoparticles. *J. Am. Chem. Soc.* **2004**, *126*, 10076–10084.
34. Ojea-Jiménez, I.; Puntes, V. Instability of Cationic Gold Nanoparticle Bioconjugates: The Role of Citrate Ions. *J. Am. Chem. Soc.* **2009**, *131*, 13320–13327.
35. Slocik, J. M.; Stone, M. O.; Naik, R. R. Synthesis of Gold Nanoparticles Using Multifunctional Peptides. *Small* **2005**, *1*, 1048–1052.
36. Krpetić, Ž.; Nativo, P.; Prior, I. A.; Brust, M. Acrylate-Facilitated Cellular Uptake of Gold Nanoparticles. *Small* **2011**, *7*, 1982–1986.
37. Nativo, P.; Prior, I. A.; Brust, M. Uptake and Intracellular Fate of Surface-Modified Gold Nanoparticles. *ACS Nano* **2008**, *2*, 1639–1644.
38. Rosi, N. L.; Giljohann, D. A.; Thaxton, C. S.; Lytton-Jean, A. K. R.; Han, M. S.; Mirkin, C. A. Oligonucleotide-Modified Gold Nanoparticles for Intracellular Gene Regulation. *Science* **2006**, *312*, 1027–1030.
39. Cheng, W.; Wang, E. Size-Dependent Phase Transfer of Gold Nanoparticles from Water into Toluene by Tetraoctylammonium Cations: A Wholly Electrostatic Interaction. *J. Phys. Chem. B* **2003**, *108*, 24–26.
40. Shen, C.; Hui, C.; Yang, T.; Xiao, C.; Tian, J.; Bao, L.; Chen, S.; Ding, H.; Gao, H. Monodisperse Noble-Metal Nanoparticles

and Their Surface Enhanced Raman Scattering Properties. *Chem. Mater.* **2008**, *20*, 6939–6944.
41. Gittins, D. I.; Caruso, F. Biological and Physical Applications of Water-Based Metal Nanoparticles Synthesised in Organic Solution. *ChemPhysChem* **2002**, *3*, 110–113.
42. Sastry, M. Phase Transfer Protocols in Nanoparticle Synthesis. *Curr. Sci.* **2003**, *85*, 1735–1744.
43. Lévy, R. Peptide-Capped Gold Nanoparticles: Towards Artificial Proteins. *ChemBioChem* **2006**, *7*, 1141–1145.
44. Puntes, V. F.; Gorostiza, P.; Aruguete, D. M.; Bastus, N. G.; Alivisatos, A. P. Collective Behaviour in Two-Dimensional Cobalt Nanoparticle Assemblies Observed by Magnetic Force Microscopy. *Nat. Mater.* **2004**, *3*, 263–268.
45. Casals, E.; Pfaller, T.; Duschl, A.; Oostingh, G. J.; Puntes, V. F. Hardening of the Nanoparticle−Protein Corona in Metal (Au, Ag) and Oxide (Fe_3O_4, CoO, and CeO_2) Nanoparticles. *Small* **2011**, *7*, 3479–3486.
46. Pujals, S.; Bastús, N. G.; Pereiro, E.; López-Iglesias, C.; Puntes, V. F.; Kogan, M. J.; Giralt, E. Shuttling Gold Nanoparticles into Tumoral Cells with an Amphipathic Proline-Rich Peptide. *ChemBioChem* **2009**, *10*, 1025–1031.
47. The measured concentration of Au^{3+} was divided by the number of gold atoms per particle to obtain the concentration of AuNPs in solution.The number of gold atoms per particle was calculated using the particle diameter, the density of bulk gold, and the molecular weight of gold; the value was 6×10^4 atoms per particle.
48. Elbakry, A.; Zaky, A.; Liebl, R.; Rachel, R.; Goepferich, A.; Breunig, M. Layer-by-Layer Assembled Gold Nanoparticles for siRNA Delivery. *Nano Lett.* **2009**, *9*, 2059–2064.
49. Laurent, S.; Burtea, C.; Thirifays, C.; Häfeli, U. O.; Mahmoudi, M. Crucial Ignored Parameters on Nanotoxicology: The Importance of Toxicity Assay Modifications and "Cell Vision". *PLoS ONE* **2012**, *7*, e29997.
50. Mahmoudi, M.; Laurent, S.; Shokrgozar, M. A.; Hosseinkhani, M. Toxicity Evaluations of Superparamagnetic Iron Oxide Nanoparticles: Cell "Vision" *versus* Physicochemical Properties of Nanoparticles. *ACS Nano* **2011**, *5*, 7263–7276.
51. Hong, R.; Han, G.; Fernández, J. M.; Kim, B.-J.; Forbes, N. S.; Rotello, V. M. Glutathione-Mediated Delivery and Release Using Monolayer Protected Nanoparticle Carriers. *J. Am. Chem. Soc.* **2006**, *128*, 1078–1079.
52. Yang, S.; May, S. Release of Cationic Polymer-DNA Complexes from the Endosome: A Theoretical Investigation of the Proton Sponge Hypothesis. *J. Chem. Phys.* **2008**, *129*, 185105–185114.
53. Jana, N. R.; Gearheart, L.; Murphy, C. J. Seeding Growth for Size Control of 5−40 nm Diameter Gold Nanoparticles. *Langmuir* **2001**, *17*, 6782–6786.
54. Based on electron diffraction studies of monolayers of alkanethiolates on Au(111) surface, which show a calculated area per molecule of 21.4 $Å^2$ (ref 39), the maximum surface density of 13 nm Au NPs would correspond to approximately 2150 AUT molecules per NP.
55. Sellers, H.; Ulman, A.; Shnidman, Y.; Eilers, J. E. Structure and Binding of Alkanethiolates on Gold and Silver Surfaces: Implications for Self-Assembled Monolayers. *J. Am. Chem. Soc.* **1993**, *115*, 9389–9401.